

Infrared Sky Brightness Monitors for Antarctica

J. W. V. STOREY, M. C. B. ASHLEY, M. BOCCAS,¹ M. A. PHILLIPS, AND A. E. T. SCHINCKEL²

Joint Australian Centre for Astrophysical Research in Antarctica (JACARA), School of Physics, University of NSW, Sydney 2052, Australia;
j.storey@unsw.edu.au

Received 1998 November 19; accepted 1999 March 8

ABSTRACT. Two sky brightness monitors—one for the near-infrared and one for the mid-infrared—have been developed for site survey work in Antarctica. The instruments, which we refer to as the NISM (Near-Infrared Sky Monitor) and the MISM (Mid-Infrared Sky Monitor), are part of a suite of instruments being deployed in the Automated Astrophysical Site-Testing Observatory (AASTO). The chief design constraints include reliable, autonomous operation, low power consumption, and of course the ability to operate under conditions of extreme cold. The instruments are currently operational at the Amundsen-Scott South Pole Station, prior to deployment at remote, unattended sites on the high antarctic plateau.

1. INTRODUCTION

The antarctic plateau is recognized as having the potential to provide some of the best astronomical observing conditions on earth (see, e.g., Burton et al. 1994). Almost all the site testing to date has been carried out at the South Pole, where it has already been demonstrated that conditions are particularly favorable for infrared and sub-millimeter astronomy. These excellent conditions arise principally from the extreme cold (down to -80°C), low precipitable water vapor (typically 250 microns in winter) and high altitude (the Pole itself is at 2841 m).

In the near-IR, Ashley et al. (1996) and Nguyen et al. (1996) report a typical sky brightness at $2.4\ \mu\text{m}$ of $100\text{--}200\ \mu\text{Jy arcsec}^{-2}$, some 50–100 times lower than at temperate sites. Ashley et al. (1996); Ashley (1998) also report fluxes at $3.5\ \mu\text{m}$ that are an order of magnitude lower. In a more comprehensive study, Phillips et al. (1999) confirm that the $2.4\ \mu\text{m}$ sky brightness can drop to as low as $50\ \mu\text{Jy arcsec}^{-2}$, with the peak of the histogram of data for the winter months occurring at a value of $150\ \mu\text{Jy arcsec}^{-2}$. They also report a reduction of a factor of 3 in the sky brightness in the “airglow dominated” region from 1 to $2.3\ \mu\text{m}$. In the mid-IR, Smith & Harper (1998) show that the South Pole again offers substantial gains, with a sky brightness as low as $35\ \text{Jy arcsec}^{-2}$ at $11.5\ \mu\text{m}$ even in summer time (“day time”).

The seeing is also found to have favorable characteristics. Although only moderately good at ground level (Loewenstein et al. 1998), the seeing is found to originate

almost entirely from the lowest 200 m of the atmosphere—leading to the possibility of using low-order adaptive optics to achieve well-corrected images over an exceptionally wide field of view (Marks et al. 1996, 1999).

Measurements at 225 GHz (Chamberlin & Bally 1994) show zenith optical depths, τ , comparable to those from the high-altitude Chilean sites in the Atacama desert that are proposed for millimeter observatories, and significantly better than at Mauna Kea, Hawaii. At 492 GHz (Chamberlin, Lane, & Stark 1997) τ is consistently low and falls below unity for weeks at a time. From the derived values of precipitable water vapor they show that the wettest quartile at the South Pole is actually drier than the driest quartile at Atacama. Lane (1998) uses these data to compute the transmission at $350\ \mu\text{m}$ and shows that the South Pole is vastly superior to Mauna Kea at this wavelength and significantly better than Atacama.

Little is known about site conditions higher on the plateau. Water vapor measurements from the Russian high-plateau site at Vostok (elevation 3488 m) have been analyzed by Townes & Melnick (1990) and suggest a significant improvement again over South Pole opacities in the sub-millimeter. Summertime measurements at Dome C (elevation 3200 m) by Valenziano et al. (1998) show not only very low precipitable water vapor values (typically $700\ \mu\text{m}$), but also very flat power spectra in the atmospheric emissivity at millimeter wavelengths—suggestive of very little boundary layer turbulence.

In order to quantify the site conditions, not just at inhabited sites such as the South Pole but also at remote, unattended locations, the AASTO experiment is being conducted. The AASTO (Automated Astrophysical Site-Testing Observatory, see Storey, Ashley, & Burton 1996; Storey 1998) is based on technology developed by Lockheed Missiles and Space for the US Automated Geophys-

¹ Present address: Cerro Tololo Inter-American Observatory, Casilla 603, La Serena, Chile.

² Present address: Smithsonian Submillimeter Array, PO Box 824, Hilo, HI 96721.



FIG. 1.—AASTO at the South Pole in 1997 January. The left-hand small box on top of the AASTO is the NISM; the box on the right is the MISM.

ical Observatory (AGO) program (Doolittle 1986) but incorporates a number of significant improvements.

The AASTO itself is a propane-powered, well-insulated shelter that keeps itself warm and generates approximately 50 watts of electrical power via a thermoelectric generator. It will eventually be equipped with a full suite of site-testing instruments, including the Antarctic Fibre-Optic Spectrometer (Boccas et al. 1998), a Differential Image-Motion Monitor (Dopita, Wood, & Hovey 1996), an acoustic sounder and the NISM and MISM (this paper).

In this paper we describe the technical issues and design characteristics of the NISM and MISM infrared sky-brightness monitors. Amongst the technical challenges is the requirement that the instrument operate unattended for up to 12 months at a time and function properly despite wind, snow, ice, and ambient temperatures as low as -80°C , while constrained to an average power budget of less than 7 watts per instrument. Figure 1 shows the AASTO at the South Pole in 1997 January, with the NISM (*left*) and MISM (*right*) in the two boxes on top of the AASTO shelter.

2. PRINCIPLE OF OPERATION

In its simplest form an infrared sky brightness monitor would consist only of a detector, together with optics that allow it to view a specified solid angle of sky. However, two improvements are possible to this basic concept that result in increased sensitivity and calibration accuracy. The first is to use an optical chopper, to mitigate the effect of the $1/f$ noise of the detector and subsequent electronics. The second is to scan the instrument in elevation, to help discriminate between flux generated by the instrument itself and true sky emission. This technique is known as “sky dipping” or “tipping.”

Clearly, it is desirable to place any chopper internal to the entrance window of the instrument, to avoid possible interference to its operation from snow or ice. However, with the chopper internal to the window, any change in window transmission (as a result of contamination, for example) might be misinterpreted as a change in sky flux. This problem can be overcome by periodically viewing a calibration target placed outside the window. The remaining problem is then that the temperature of the chopper blade must be accurately known, as it is the *difference* in temperature between the chopper blade and the sky that forms the basis of the measurement. Unfortunately, direct measurement of the rotating chopper blade is impossible, so it can only be inferred from the temperature of nearby objects in the optics box.

An additional issue concerns dynamic range. Ideally, the sky should be chopped against a blackbody of comparable flux. However, with the sky emissivity as low as 1% at some wavelengths, this would require that the blackbody temperature be well below ambient—necessitating some kind of cryogenic system that would inevitably be both complicated and power hungry.

The solution adopted here is to use a reflective chopper wheel and appropriate optics to allow the detector to chop between two patches of sky separated by 45° in elevation. The entire instrument is then scanned in elevation to produce the familiar “sky dip.” A blackbody source is placed external to the instrument in such a position that it fills one of the beams when the other beam is at 45° elevation.

The basic observing sequence is shown in Figure 2. With the beams placed symmetrically either side of the zenith (*a*), the flux should be zero. In practice it is not; a small offset v_1 results from imbalances between the two optical paths and is simply subtracted from each subsequent measurement.

In position (*b*), Beam A is at the zenith and Beam B at 45° elevation. If the emission from the atmosphere has a $\sec \theta$ dependence (where θ is the zenith angle), the flux in Beam B should now be $\sqrt{2}$ times the flux in Beam A. Let the signal from the detector here be v_2 . (Note that the validity of the $\sec \theta$ dependence can itself be checked by observing at a range of other elevations.)

Finally, in position (*c*), Beam B sees the blackbody and Beam A is at 45° elevation; let the measured signal here be v_3 .

It is straightforward to show that the flux from the sky at the zenith can be expressed in terms of the flux from the blackbody as

$$F_{\text{sky}}/F_{\text{bb}} = \frac{v_2 - v_1}{\sqrt{2}(v_2 + v_3) - (v_3 - v_1)}.$$

It is also tacitly assumed that the detector output current (which is converted to voltages v_1 , v_2 , and v_3 by a transim-

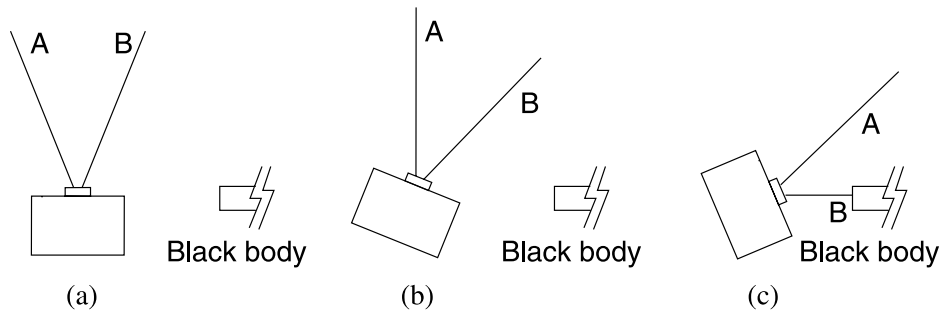


FIG. 2.—Basic observing sequence. The instrument chops between two beams (labeled A and B) separated by 45° in elevation. See text for details.

pedance amplifier) is a linear function of the infrared power incident on the detector. This is generally true, but the extent to which it is not is another reason for wanting to keep the dynamic range of signals through the system as low as possible.

In principle the instruments could have been made smaller, cheaper, and less power hungry by combining them into a single package. Considerations of flexibility and redundancy, however, favor two separate instruments.

3. OPTICS

The layout of the MISM is shown in Figure 3. The detector looks out through a cold stop that defines the f -ratio. A pair of lenses images the detector onto an ambient-temperature filter wheel. The beam then expands to a further lens, which reimages the detector onto the reflective chopper wheel. From the chopper wheel the two beams expand to give the two 4° cones on the sky. The chopped beams cross as they pass through the window, with the

result that any build-up of ice crystals on the window should affect both beams equally. The entrance window and all lenses are of AR-coated ZnSe.

The chopper wheel is fabricated from 1.0 mm thick stainless steel sheet using a chemical etching process and has 30 teeth to reduce the rotational speed required to achieve the necessary chopping frequency of 1 kHz. It is coated with an evaporated gold layer to ensure good IR reflectivity.

All of the beam-steering mirrors are of gold coated Pyrex. The overall transmission from sky to detector is estimated at 50%, including the bandpass filter or CVF.

Provision is made to electrically heat the entrance window to drive off any ice that might accumulate there. However, no evidence has been found that there is any ice accumulation at all. Holding the window slightly above ambient temperature, combined with the clean shape of the instrument (see § 7), appears to be all that is required to prevent ice build-up.

The MISM filter wheel contains the following filters:

1. A standard astronomical “N” filter (8.07 to $13.3 \mu\text{m}$);

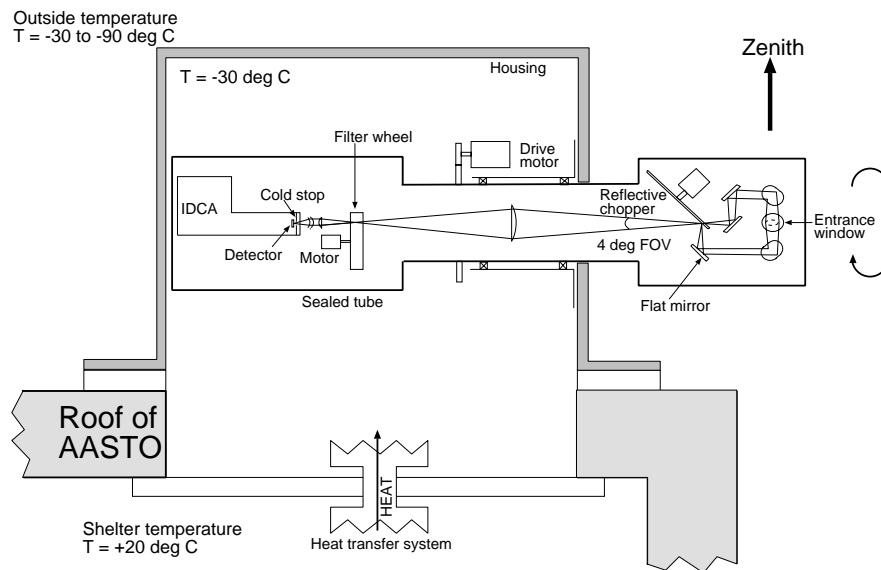


FIG. 3.—Optical layout of the MISM

2. A circular variable filter (CVF) covering 4.3 to 7.7 μm at a resolving power of $\lambda/\Delta\lambda = 74$;
3. A CVF covering 7.7 to 14.1 μm at $\lambda/\Delta\lambda = 55$;
4. A narrowband filter covering 10.6 to 11.3 μm , allowing sensitive measurements to be made in "Craig band," a region of particularly low sky brightness reported by Smith & Harper (1998).

The NISM is similar to the MISM but somewhat simpler, as there is no filter wheel. Instead, a cold bandpass filter, nominally covering 2.27 to 2.45 μm (the " K_{dark} " window), is attached to the cold stop inside the Stirling cooler. A single, positive meniscus lens of AR-coated ZnSe forms an image of the detector onto the four-bladed chopper wheel. Thereafter the optical train is identical to that in the MISM, except that the entrance window is AR-coated sapphire.

4. DETECTOR AND COOLER

The detectors are cooled to cryogenic temperatures by miniature Stirling-cycle coolers. These units, known as integrated detector/cooler assemblies (IDCAs) are common in aerospace applications, but we are unaware of their previous use in ground-based astronomy. Their advantages include very low power consumption, reliable operation and, of course, freedom from the tyranny of cryogenic liquids.

The NISM detector is a 2 mm diameter InSb photodiode from Cincinnati Electronics, integrated into a Ricoh K518A cooler. The detector operating temperature is 90 K. A Cincinnati Electronics AM300 transimpedance preamplifier is located in the detector box as close as possible to the cooler. This provides sufficient gain to minimize subsequent interference. The signal is then sent down to the AASTO electronics rack via shielded, twisted-pair cable.

The MISM detector is a 0.25 mm square HgCdTe photoconductor from the Judson J15D4 series, with a peak responsivity at $\lambda = 13 \mu\text{m}$ and a cutoff wavelength beyond 14 μm . It is integrated into an Inframetrics RC-1 cooler, which brings it down to an operating temperature of 77 K. A Judson PA101 preamplifier is mounted immediately adjacent to the cooler.

Both coolers require just a few watts to cool the detectors to operating temperature within about three minutes. Once cold, the coolers throttle back to an even lower steady state power consumption—in the case of the MISM just 2.5 watts.

5. ELECTRONICS

The electronics is designed to be as simple as possible, be reliable, and have low power consumption. Some of the novel or unusual features are detailed below.

Signal chain.—After passing through the preamplifiers in the detector box, the signal passes to the AASTO electronics rack. There, it is further amplified, then sent through an active bandpass filter with a Q of 10. It is then sampled by an A/D converter for subsequent synchronous demodulation in software.

Chopper.—Because the chopper motor must run reliably for long periods, a brushless design is required. However, the motor must also run at temperatures that may fall to -90°C —well below the rated temperature of normal Hall-effect sensors. For this reason, we chose to use a sensorless design, in which the instantaneous rotor position is calculated from the back-emf generated in the stator windings. The model chosen is an ESCAP 26BC-3C three-phase motor. The chopper phase is sensed optically; this signal is also used to phase lock the chopper to a computer-generated reference frequency. Power consumption of the chopper and drive electronics is approximately 0.5 watts.

Phase locking of the chopper, and thereby forcing it to operate at a precisely determined frequency, has two advantages. First, the frequency can be chosen to avoid the noise spikes that are generated by the cooler motor at harmonics of its operating frequency. Second, the signal chain can then include reasonably high- Q tuned filters, greatly reducing the dynamic range requirements on the A/D converter and digital signal processing systems.

The NISM chopper runs at 77 Hz, while the MISM is operated at 1 kHz. The higher frequency of the MISM is dictated by the higher $1/f$ noise corner frequency of the HgCdTe detector.

Stepper motor.—The entire instrument is scanned in elevation by rotating it around a horizontal axis. An ESCAP model P352 stepper motor with cold-rated K40 reduction gearbox drives a ring gear via a small pinion. A similar but smaller stepper motor is used in the MISM to rotate the filter wheel. The stepper motor drivers are of the "chopper" variety to maximize efficiency, with a switching frequency of about 30 kHz.

Power supplies.—The instruments are powered by sealed lead-acid batteries, which in turn are charged via current-limited galvanically isolated switching power supplies from the AASTO 28 volt bus. All power is then derived from the batteries via switching power supplies operating at very high efficiency (typically 90%–98%). The power supplies are activated only when required. Power switching is done using high-side MOS switches (rather than relays) to reduce power and enhance reliability.

Computer.—The instrument control and data-acquisition computer for each instrument is a built around a set of cards conforming to the PC/104 standard. The CPU card is manufactured by DSP and is based on a 486 processor. A 12-bit A/D card by Diamond Systems control most of the functions of the instrument, samples the data and monitors important functions of the instrument. The software for the

two instruments runs under the real-time multitasking operating system RTKernel. At the present time we are not using the AASTO's DAU and DCU computers except for monitoring and housekeeping.

6. CALIBRATION

The instruments require only a single flux calibrator. As is traditional in infrared astronomy, this takes the form of a blackbody source. A massive piece of OFHC copper bar (100 mm diameter \times 300 mm long) has a part-cylindrical, part-conical cavity machined in each end—one for the NISM and one for the MISM. These cavities are painted with Ames 24E2 IR-black coating (Smith 1991), which should have an emissivity of better than 99% at these wavelengths. (The overall emissivity of the blackbody source is of course much higher because of the shape of the cavity.)

The copper bar is well insulated and is thermally coupled by a substantial copper rod to the inside volume of the AASTO, where it taps into the warmth of the building air via a large finned heat sink (in this case a "heat source"). By this means the blackbody calibrator is kept at between 10 and 30 K (depending largely on wind speed and direction) above the outside ambient air temperature. Platinum resistance thermometers monitor the temperature of the blackbody with an absolute accuracy of about 0.1 K.

Because the blackbody source fills the beam of each instrument, the exact value of the beam solid angle cancels out of the calculation of sky brightness per unit solid angle. Ultimately, values of sky brightness we report are ratios of the flux from the sky to that from our blackbody.

7. MECHANICAL CONSTRUCTION

Each instrument comprises two boxes—an optics box and a detector box—joined by a length of aluminum tube. Each box is fabricated by welding aluminum plates together. In each box, one plate has a machined surface that acts as the single mounting face for all of the optical components. The instrument is then fully sealed, with fluorosilicone o-rings used to ensure vacuum integrity even at very low temperatures. As with the AFOS (Boccas et al. 1998), a small canister containing about 50 grams of calcium hydride is incorporated into the sealed interior volume of each instrument. Calcium hydride is a particularly aggressive dessicant, capable of competing successfully for water vapor with the cold surfaces such as the entrance window (Schriver 1969).

The instruments are insulated with foam/fiberglass sandwich and placed atop the 16 inch diameter roof ports of the AASTO. There, room heat from the AASTO can keep the inside of the detector box (which contains the Stirling cooler, preamplifier and other temperature sensitive

components) at a temperature well above the outside ambient.

In the case of the MISM, some sensitivity gains can be expected by allowing the majority of the optics (and in particular the filters) to cool to about -30 °C; a limit imposed by the Stirling cooler and electronic components. To achieve this, the MISM is not coupled directly to the warm interior of the AASTO. Instead, a self-regulating methanol-filled heat pipe, manufactured by Thermacore, is interposed between it and the AASTO.

To generate a sky-dip the instruments are rotated along the axis of the tube that joins the optics box to the detector box. Oversize ball races, degreased and relubricated with low-temperature teflon-filled lubricant are used. Two types of seal are employed. The ball races themselves have an inner seal of felt, while the gap between the optics box and detector box has an outer seal consisting of long brushes made from horse tail hair.

The entrance windows are elevated above the aluminum surface of the optics boxes on small towers. This brings them flush with the outer surface of the fiberglass insulating cover. The polished surfaces of the fiberglass cover, together with the almost complete absence of any step between the cover and window, is an important factor in minimizing the build-up of wind-borne ice and snow.

8. PERFORMANCE

The NISM sensitivity is limited by Johnson noise in the feedback resistor of the detector preamplifier. This resistor is uncooled and is external to the IDCA; increasing its value above the 22 M Ω we chose was found to make the system unduly sensitive to interference. The sensitivity achieved is approximately 100 μ Jy arcsec $^{-2}$ Hz $^{1/2}$.

The MISM sensitivity is limited by the excess noise of the detector itself. As a result the sensitivity is linearly related to the infrared bandpass of the filter used, ranging from 25 mJy arcsec $^{-2}$ Hz $^{1/2}$ with the broadband "N" filter to 1 Jy arcsec $^{-2}$ Hz $^{1/2}$ with the CVF.

The NISM and MISM were deployed to the South Pole in 1997 January. Both instruments have suffered from some teething difficulties, and data taking has been hampered by the failure of the AASTO power system early in each of the 1997 and 1998 seasons. We present here only preliminary results; at the time of writing data taking is still in progress, and a thorough analysis of the data is underway.

Figure 4 shows the demodulated detector output signal from the NISM as a function of elevation, i.e., a "sky dip." In this case θ is defined as the elevation angle, relative to the "counterclockwise" horizon, of a point midway between the two beams. That is, beam A is at an elevation of $\theta - 22.5$; Beam B is at $\theta + 22.5$ relative to this horizon. The solid line shows the actual data from 1997 January; the dotted line is a theoretical curve assuming a $\sec \theta$ emissivity

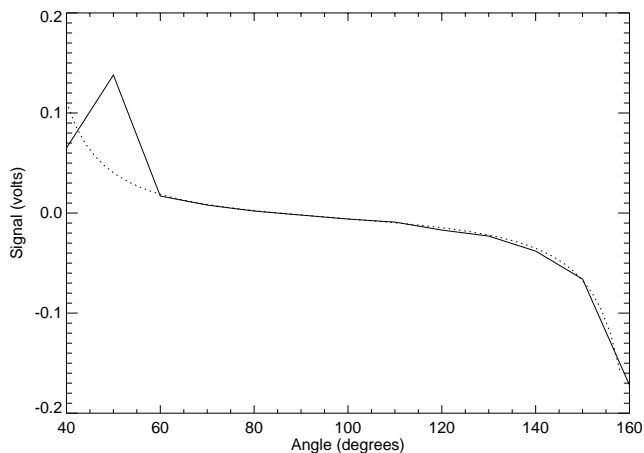


FIG. 4.—Output signal from the NISM as a function of elevation, i.e., a “sky dip.” The solid line shows the actual data from 1997 January; the dotted line is a theoretical curve assuming a $\sec \theta$ emissivity dependence. The calibration blackbody is to the left of the NISM, and so the signal from this calibrator appears near the “anticlockwise” horizon.

dependence. The calibration blackbody is to the left of the NISM, and so the signal from this calibrator appears near the “anticlockwise” horizon.

Figure 5 shows similar sky dip data for the MISM. In this case the different curves represent the results from the different infrared filters. The calibration blackbody source is to the right of the MISM, and so the peak from the blackbody appears near the “clockwise” horizon. The “step” at about 150° is caused by one of the beams hitting the blackbody housing. Similarly, the abrupt change in flux below 40° is the result of the lower beam seeing the AASTO support legs and, eventually, the snow.

In Figure 6 the CVFs have been scanned through their range, at appropriate elevation angles as described in § 2, to

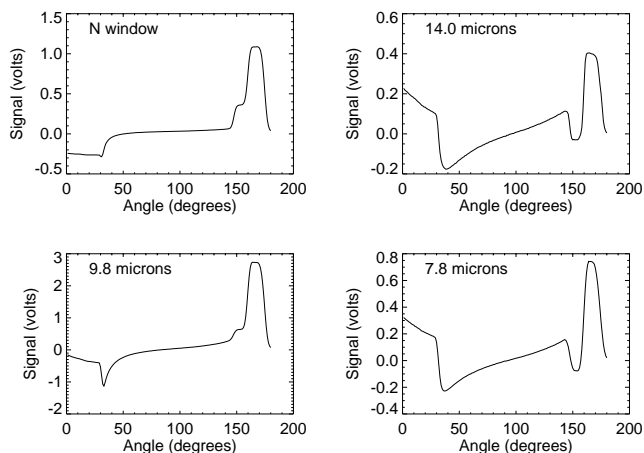


FIG. 5.—Sky-dip data for the MISM. The different curves represent the results from the different infrared filters. The calibration blackbody source is to the right of the MISM, and so the peak from the blackbody appears near the “clockwise” horizon.

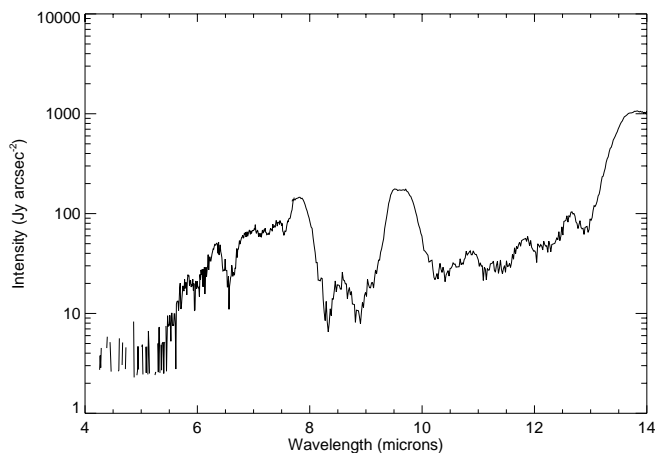


FIG. 6.—Mid-infrared sky emission as measured by the MISM. The “*N*-band” atmospheric window from 8 to $14 \mu\text{m}$ can clearly be seen, bisected by the strong emission lines of stratospheric ozone at around $9.7 \mu\text{m}$. Note that the apparent “window” at $6.5 \mu\text{m}$ is an artifact caused the very high optical depth of the atmosphere at this wavelength.

generate a spectrum of the sky emission. The “*N*-band” atmospheric window from 8 to $14 \mu\text{m}$ can clearly be seen, bisected by the strong emission lines of stratospheric ozone at around $9.7 \mu\text{m}$.

By sitting at a fixed elevation and wavelength and sampling the data continuously, the stability of the sky emission can be determined. This is shown in Figure 7, where the upper plot is the raw time series and the lower is the computed power spectrum derived from the time series via a Fourier transform.

9. CONCLUSION AND FUTURE PLANS

The NISM and MISM have achieved their design goals of automatically acquiring sky-brightness measurements

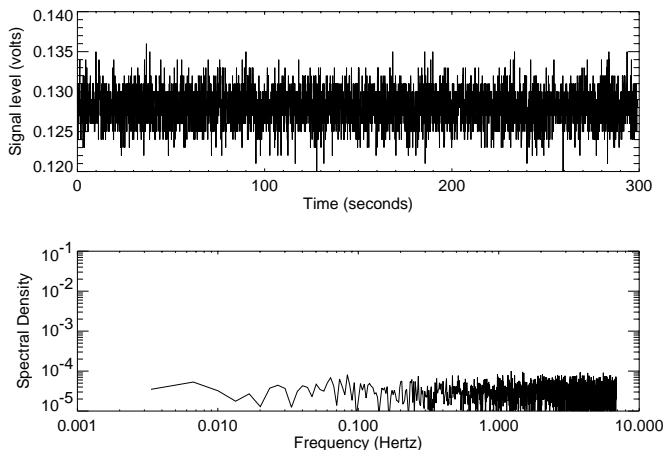


FIG. 7.—Temporal stability of the mid-infrared sky measured by the MISM. The upper plot is the raw time series, and the lower is the computed power spectrum derived from the time series via a Fourier transform.

under antarctic conditions. The MISM has been particularly successful, carrying out the first comprehensive study of the winter-time mid-infrared sky from the South Pole (Chamberlain et al. 1999).

At present both instruments are controlled via the Internet, using either automated scripts residing on a Unix workstation, or by direct human intervention. When the AASTO moves away from the South Pole, real-time Internet control will no longer be possible. We are currently exploring two avenues for remote operation.

1. Fully automated operation, in the manner of the instruments deployed in the Automated Geophysical Observatories, with data recorded on disk and retrieved only once per year. Only health and status data will be available in near real-time via an ARGOS satellite link.

2. Implementation of a real-time two-way communications channel, or a two-way "store and forward" system, using low earth orbit polar-orbiting satellites.

One (or possibly both, for redundancy) of these systems will need to be in place to prepare the AASTO for field deployment in 1999 or 2000.

This research is supported by an Australian Research Council grant and by a DIST travel grant. The AASTO itself was funded through University of NSW and Australian National University discretionary grants and is deployed at the South Pole as part of our collaboration with the Center for Astrophysical Research in Antarctica under NSF grant OPP 89-20223. We particularly thank Paul Sullivan and Robert Schwartz, who were the winter-over support staff assigned to the AASTO in 1997 and 1998, respectively. Successful construction of the NISM and MISM was only possible because of the skill and dedication of the workshop staff at UNSW. We also thank Matt Chamberlain for his preliminary reduction of the MISM data and preparation of the figures, and Michael Burton for his enthusiasm, encouragement, and advice in the development of these two instruments.

REFERENCES

- Ashley, M. C. B. 1998, in ASP Conf. Ser. 141, *Astrophysics from Antarctica*, ed. G. Novak & R. H. Landsberg (San Francisco: ASP), 285
- Ashley, M. C. B., Burton, M. G., Storey, J. W. V., Lloyd, J. P., Bally, J., Briggs, J. W., & Harper, D. A. 1996, *PASP*, 108, 721
- Boccas, M., Ashley, M. C. B., Phillips, M. A., Schinckel, A. E. T., & Storey, J. W. V. 1998, *PASP*, 110, 306
- Burton, M. G., et al. 1994, *Publ. Astron. Soc. Australia*, 11, 2
- Chamberlain, M., et al. 1999, in preparation
- Chamberlain, R. A., & Bally, J. 1994, *Appl. Opt.*, 33, 1095
- Chamberlain, R. A., Lane, A. P., & Stark, A. A. 1997, *ApJ*, 476, 428
- Doolittle, J. H. 1986, Lockheed Tech. Mem. LMSC-F171145
- Dopita, M. A., Wood, P. R., & Hovey, G. R. 1996, *Publ. Astron. Soc. Australia*, 13, 39
- Lane, A. P. 1998, in ASP Conf. Ser. 141, *Astrophysics from Antarctica*, ed. G. Novak & R. H. Landsberg (San Francisco: ASP), 289
- Loewenstein, R. F., Bero, C., Lloyd, J. P., Mrozek, F., Bally, J., & Theil, D. 1998, in ASP Conf. Ser. 141, *Astrophysics from Antarctica*, ed. G. Novak & R. H. Landsberg (San Francisco: ASP), 296
- Marks, R. D., Vernin, J., Azouit, M., Briggs, J. W., Burton, M. G., Ashley, M. C. B., & Manigault, J. F. 1996, *A&AS*, 118, 385
- Marks, R. D., Vernin, J., Azouit, M., Manigault, J. F., & Clevelin, C. 1999, *A&A*, 134, 161
- Nguyen, H. T., Rauscher, B. J., Severson, S. A., Hereld, M., Harper, D. A., Loewenstein, R. F., Mrozek, F., & Pernic, R. J. 1996, *PASP*, 108, 718
- Phillips, M. A., Ashley, M. C. B., Burton, M. G., Storey, J. W. V., Lloyd, J. P., Harper, D. A., & Bally, J. 1999, *ApJ*, submitted
- Schrifer, D. F. 1969, *The Manipulation of Air Sensitive Compounds* (London: McGraw-Hill)
- Smith, C. H., & Harper, D. A. 1998, *PASP*, 110, 747
- Smith, S. M. 1991, *NASA Tech. Mem.* 102864
- Storey, J. W. V. 1998, in ASP Conf. Ser. 141, *Astrophysics from Antarctica*, ed. G. Novak & R. H. Landsberg (San Francisco: ASP), 313
- Storey, J. W. V., Ashley, M. C. B., & Burton, M. G. 1996, *Publ. Astron. Soc. Australia*, 13, 35
- Townes, C. H., & Melnick, G. 1990, *PASP*, 102, 357
- Valenziano, L., et al. 1998, in ASP Conf. Ser. 141, *Astrophysics from Antarctica*, ed. G. Novak & R. H. Landsberg (San Francisco: ASP), 81